Journal of Neonatal Surgery
ISSN(Online): 2226-0439
Vol. 14, Issue 17s (2025)
https://www.jneonatalsurg.com

OPEN ACCESS

Development and Assessment of Solid Lipid Nanoparticles of Bergamot Essential Oil

Gaurav Mude[1], Shantilal Singune[1]

[1]Institute of Pharmaceutical Sciences, SAGE University, Indore (MP), India-452020

Cite this paper as: Gaurav Mude, Shantilal Singune, (2025) Development and Assessment of Solid Lipid Nanoparticles of Bergamot Essential Oil. *Journal of Neonatal Surgery*, 14 (17s), 61-84.

ABSTRACT

Bergamot essential oil (BEO) administration by Solid Lipid Nanoparticles (SLNPs) is an innovative approach to improving the therapeutic potential and stability of the oil. Unfortunately, bergamot essential oil has a number of drawbacks, including a high volatility, low solubility, and a vulnerability to environmental deterioration, despite its well-known antibacterial, antioxidant, and anti-inflammatory characteristics. An intriguing option is SLNPs, which encase BEO in a lipid matrix and provide advantages such as controlled release, increased bioavailability, and protection from environmental influences. The researchers in this work used a heated homogenization and ultrasonication technique to create SLNPs that contained BEO. Size, shape, encapsulation effectiveness, zeta potential, and polydispersity index (PDI) were the parameters measured for the nanoparticles. Verification of physicochemical stability was carried out using differential scanning calorimetry (DSC) and Fourier-transform infrared spectroscopy (FTIR), which showed that BEO was successfully encapsulated and was compatible with the lipid matrix. A prolonged release profile was shown in in vitro release tests, which greatly reduced the evaporation of volatile chemicals. In comparison to free BEO, SLNPs loaded with BEO showed improved efficacy against common pathogens in antimicrobial tests. Tests for cytotoxicity validated the compositions' biocompatibility, lending credence to their medicinal promise. In light of the shortcomings of BEO, this study demonstrates the effectiveness of SLNPs, opening the door for their use in the food, cosmetic, and pharmaceutical sectors. Additional in vivo investigations into the feasibility and therapeutic use of SLNPs as a vehicle for bergamot essential oil administration are warranted in light of these results.

Keywords: *Solid Lipid Nanoparticles (SLNPs), Bergamot Essential Oil (BEO), Nanoencapsulation, Controlled Release, Antimicrobial Activity*

1. INTRODUCTION

1.1 Background and Significance of Bergamot Essential Oil (BEO)

Citrus classification and labelling are complex and have changed significantly in recent years (refer to Table 1). For over four centuries, botanists have faced challenges in pinpointing the center of origin and phylogeny of Citrus species. These challenges stem from the species' unique reproductive characteristics, cultural and geographic influences, and advancements in phylogenetic analysis techniques, which have led to shifts in classification over time [1].

The entire Citrus plant, known for its fragrant flowers, leaves, and fruits, has captivated humanity for thousands of years. Citrus species have been cultivated and selectively bred since ancient times. Classical Chinese texts from the second millennium BCE mention domesticated mandarins and pomelos, while citrons are depicted on the walls of Egypt's Karnak Temple, which dates back 3,000 years. Citrus fruits were also integral to ancient civilizations in India, Japan, Mesopotamia, Persia, Media, Palestine, Greece, and Rome, as well as within Jewish culture. During the medieval era, the Arabs further advanced the cultivation of various Citrus species, introducing agronomic innovations and spreading the plants across numerous regions [2].

Citrus evolution in Asia and Europe was complicated. This process has produced numerous interspecific hybrids and cultivars, complicating morphology-based classification. Genetically distinct fruits may seem alike, whereas genetically comparable cultivars may have very diverse morphologies [1,3].

Citrus species are also highly prone to spontaneous mutations and hybridization, often crossing with parent species to create creatures that share a common ancestry yet morphologically distinct, or vice versa. Consequently, many commonly consumed Citrus fruits today are hybrids rather than true species (see Table 2) [4]. Additionally, some Citrus species reproduce through apomixes a type of asexual reproduction via maternal nucellar embryogenesis. This process results in polyembryony seeds containing clonal embryos derived solely from maternal tissue, without genetic contributions from a second parent, as opposed to two-parent zygotic embryos. Apomixis slows or halts evolutionary processes, further complicating taxonomy based on morphological traits and obscuring the true lineage of Citrus species [5, 6].

Table 1: The taxonomy and classification complexities of the Citrus genus [7]

Aspect	Description
Taxonomic Challenges	Rapidly changing taxonomy and nomenclature due to evolving phylogenetic techniques
Reproductive Features	High frequency of spontaneous mutations and hybridization
Domestication and Cultivation	Ancient cultivation in China, India, Egypt, Persia, Greece, Rome, and spread by Arabs during the Medieval era
Morphological Complexity	Similar morphology in genetically distant species; differing morphology in genetically close varieties
Hybridization	Creation of hybrids through natural and artificial processes; hybrids often re-crossed with parent species
Reproductive Modes	- **Apomixis**: Maternal nucellar embryogenesis produces clonal embryos
	- **Zygotic Embryogenesis**: Mono-embryonic seeds with genetic material from both parents
Challenges for Phylogeny	Difficult to trace clear genealogies due to reproductive modes and hybridization
Domestication Process	Led to high numbers of interspecific hybrids and cultivars, complicating taxonomy

1.1.1 Origins of the Genus Citrus

In his groundbreaking work Species Plantarum, Carl von Linné (Linnaeus) categorized the Rutaceae Citrus genus. Citrus medica L., often known as lemons, and Citrus aurantium L., well known as bitter oranges, comprise the two main groups of citrus fruits according to Linnaeus. Botanists recognized several species after this morphological and geographical classification [8]. The taxonomy of Citrus experienced a substantial alteration due to the introduction of molecular laboratory techniques [9].

Research has identified ten progenitor species of Citrus, seven of which originate in Asia. Recent genomic studies, using single nucleotide polymorphism (SNP) analysis, have provided insights into the evolutionary relationships within the genus [10]. The Citrus clade includes Fortunella, Eremocitrus, and Microcitrus, according to this research. Citrus maxima, reticulata, and medica are the original species that produced the principal hybrids: Lemons, limes, oranges, grape fruitS [11].

Modern dispersion implies central-southern China is the biological core, followed by southeast Himalaya and southern China. The migration of **Citrus** to areas such as Malaysia and Australia are thought to have occurred during the Miocene/Pliocene period [12, 13]. Given the intricate taxonomy of the **Citrus** genus, agronomic classification is often employed for commercially significant species. This approach organizes cultivars into eight main groups based on agronomic traits. This practical framework simplifies identification and classification for agronomic and commercial purposes [14, 15].

1.1.2 Taxonomic Classification of Bergamot

Bergamot (Figure 1)'s past evolution and nomenclature are notably problematic because to its uncertain origin.

Figure 1. The Bergamot plant and its fruit

Bergamot is an interspecific hybrid, evidenced by its high degree of heterozygosity [8], and it have been classified alongside Bitter Orange [16,17]. Citrus clade phylogeny suggests bergamot developed late and was not mentioned by ancient authors. Some sources say this hybrid evolved in Calabria or southern Italy [18], while others say it evolved in the Antilles, Greece, or Canary Islands before being transferred to Calabria [18]. One theory posits that Columbus brought the hybrid to Italy via the Spanish city of Berga, inspiring the name "Bergamot" [19].

1.2 Limitations of BEO in Therapeutic Applications

BEO has a vast-standing history in Italian folk medicine, where it has been traditionally utilized in handcrafted and homemade formulations for topical applications. These preparations were commonly employed as antiseptics for skin disinfection and to aid in the healing of minor wounds. Although BEO is generally well absorbed, its photosensitive properties, attributed to the existence of furocoumarins such as 5-MOP, have raised safety concerns. In response, psoralen-free versions of BEO have been developed and are recommended for topical use to minimize the risk of phototoxicity. Despite its extensive historical use, details of phototoxic reactions to BEO, particularly in aromatherapy applications, remain relatively rare [20].

BEO has shown several biological actions, including antibacterial, anti-inflammatory, antiproliferative, and analgesic capabilities, along with influences on the body functions. These findings suggest promising potential for clinical applications in the future. However, to date, most clinical studies have focused on the aromatherapy benefits of BEO, primarily investigating its anxiolytic effects and ability to reduce stress responses. These studies suggest that BEO could be effective in managing anxiety and mitigating stress-related effects through aromatherapy treatments [20].

1.3 Bergamot Essential Oil SLNPs as a Novel Delivery System

Nanoemulsions (NEs) are characterized as heterogeneous systems consisting of two immiscible liquids spread inside each other, with emulsion particle sizes generally under 1000 nm [21]. In actuality, the mean particle size typically ranges from 100 to 500 nm, with the majority of NEs displaying particle sizes between 20 and 200 nm and a narrow size distribution [21, 22]. NEs are categorized into two principal types: oil-in-water (o/w) emulsions and the inverse water-in-oil (w/o) emulsions [23]. In contrast to traditional emulsions, which have a milky or opaque appearance, nanoemulsions are frequently characterized as translucent or transparent [24].

Nanoparticles exhibit several advantageous properties, such as diminutive particle size, elevated surface area and the possibility for site-specific or targeted administration. These attributes have made NEs a popular choice in drug delivery systems, dietary supplements, and cosmetic formulations [26]. Ultrasound, high-pressure areas homogenization, inversion of phase temperature, and emulsified inversion point technologies are used to prepare them [27]. Recent articles address NEs' physical properties, composition, and preparation.

1.3.1 Encased in Liposomes: Essential Oils

Liposomes are microscopic artificial vesicles with a lipid bilayer and a distinct compartment. They are usually manufactured from either synthetic or natural phospholipids with cholesterol to stabilize the membrane. Liposomes can be prepared using methods such as extrusion, injection, or microfluidics. Chemically, liposomes consist of phospholipids, particularly phosphatidylcholine. The external surface of the liposome may also feature ligands that help the liposome recognize and be accepted by specific tissues. Liposomes are multilamellar, tiny unilamellar, or large unilamellar, with the number of concentric membranes depending on development, but bilayer or monolayer membranes are the most prevalent [28, 29, 30].

1.3.2 Essential Oils Encapsulated in Solid Lipid Nanoparticles

SLNPs are oil-in-water emulsions with a solid lipid phase at room temperature, permitting hydrophilic and hydrophobic molecules [31, 32]. Elkordy et al. [33] reviewed therapeutically active natural product extract pharmaceutical formulations. Gupta et al. [34] discussed phyto nano formulations that offer controlled release of active ingredients, enhancing their immersion at pancreatic cancer sites, thus improving therapeutic outcomes for cancer cells. Nano formulations based on vegetable oil-derived bioactive compounds have shown improved uptake, absorption, and bioavailability, contributing to disease prevention and management. Yap et al. examined the medication delivery of natural goods, encompassing extracts and essential oils (EOs) from 9 medicinal plants, using nanocarriers to improve breast cancer therapy [35].

2. MATERIALS AND METHODS

Standard Calibration Curve

Drug Excipients Interaction Study:

FTIR: FTIR spectroscopy is a fundamental analytical technique employed to acquire the infrared spectrum of various substances, including solids, liquids, and gases. FTIR spectrometers can collect high-resolution data across a wide wavelength range. This gives it an edge over dispersive spectrometers, that can only detect intensity across a limited spectrum window. FTIR is resilient and powerful in scientific research and industrial applications as it simultaneously collects broad-spectrum data to improve spectral analysis.

The FTIR spectrum's major purpose was to serve as a study for the manufactured SLN and pure medication, allowing them to be compared for any potential incompatibility. A 1:1 combination of medication and excipients was made and combined with the appropriate amount of potassium bromide. About 100mg of this combination was compacted into a pellet. An FT-IR spectrophotometer was used to scan it from 4000 to 150 cm-1. Looking for peak elimination or the growth of a new biological category, the infrared spectra of the physical combination were compared to the standard value of pure drug and excipients.

DSC: DSC is a thermo-analytical method that quantifies the differential heat necessary to elevate the temperature of the specimen compared to a standard as an estimate of temperature. Sample and reference are kept at similar temperatures during the experiment. The DSC analysis temperature methodology usually ensures that the sample holder's temperatures rise linearly. The sample being studied must have a specified thermal capacity throughout the temperature range to be investigated. DSC measures the level of heat received or released via physical transformations, such as phase transitions. The quantity of heat required depends on the exothermic or endothermic process. For example, solid samples require more heat to increase their temperature, while exothermic processes require less heat. DSC is utilized in industry for quality assurance, sample purity, and polymer curing analyses. The DSC thermograms of the Essential Oil and its prepared SLN were recorded using differential scanning calorimetry DSC Universal Q20 V24.10 Build 122 TA instrument. 20 mg of both samples were used from the range of 10^{o}C to 420^{o}C at a rate of 10^{o}C/min. The DSC spectra of the samples are shown in ***Fig No. 4 and 5*** respectively.

X-Ray Diffraction (XRD): These techniques rely on the scattering of X-rays by crystalline structures. These approaches enable the identification of the crystal structures of diverse solid substances. These approaches are far more essential than X-ray absorption and X-ray fluorescence techniques. X-ray diffraction techniques are often used to examine interior structures. The X-ray diffractogram of the pure Essential Oil drug and its prepared SLN were recorded between 2°–50° (2θ) at room temperature using X-ray diffractometer. Using a Cu-Ka radiation source, specimens were scanned at 5°/minute across a 2θ range of 2°–50°. The diffractograms of pure Essential Oil is shown in Figure 6 and its peaks in Table 3 while on the other hand the diffractograms of prepared SLN can be seen in Figure 7 and its peaks in Table 4.

Scanning Electron Microscope (SEM): SEMs employ a focussed electron beam to scan a sample's surface. Various signals from the sample's atoms and electrons reveal the structure and surface topography. After a raster scan sequence, the electron beam position and signal strength generate a picture. In the main scanning electron microscopy mode, an Everhart-Thornley detector detects secondary electrons generated by atoms stimulated by the electron beam. The specimen's topography affects secondary electron detection and signal strength as SEM resolution exceeds 1 nm.

Transmission Electron Microscopy (TEM): The morphology of FMO-SLNs was investigated using a JEM-1230 transmission scanning electron microscope (JEOL, Tokyo, Japan). Samples were placed on a film-coated gold grid after dilution. After applying 2% phosphor tungstic acid to the film, it was left to cure for 10 minutes before inspection.

Particle Size Measurement: Pharmaceutical manufacturing materials depend on the active ingredient and excipient property. Particle size, distribution, and shape affect bulk characteristics, product efficiency, processability, stability, and form. It is well known that particle size affects product dissolving, absorption, and content homogeneity.

Determination of residual solvent by Head space gas chromatography: To avoid the possible health hazards linked to excessive exposure to this chemical compound, the International Council for Harmonization advises that daily intake of

chloroform, regardless of method, should not exceed 60 parts per million (PPM).

Optimized agglomerates that had been precisely weighed were suspended in methanol and agitated for 24 hours at 100 rpm in an orbital shaking incubator. After filtering the dispersion, the filtrate was subjected to HS-GC analysis utilizing column Rtx-5MS with helium as the carrying gas. The solvent concentration in SLNs was calculating peak area that was formed when HS-GC was alternatively injected with 1000 ppm reference and sample solutions.

Calculation of Lambda Max: For the purpose of determining the maximum absorption of the essential oil pure drug, an initial step involved dissolving 50 mg of the drug in 50ml of methanol. This solution was then subjected to sonication and subsequently analyzed using a double beam UV Spectrophotometer. The maximum absorbance, a crucial measurement in this experiment, was detected at a wavelength of 254nm, providing essential information for the ongoing research study.

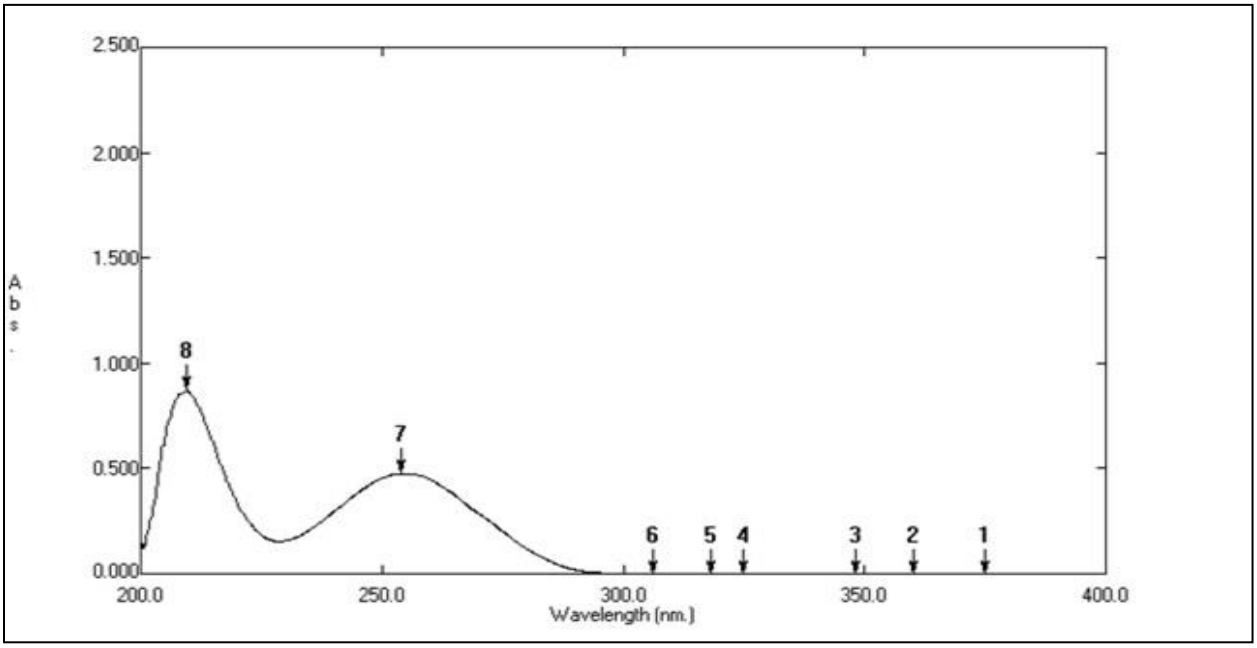

Figure 2: Maxima Absorption of Essential Oil in Methanol

Preparation of standard calibration curve:

Essential Oil pure drug (50 mg) was carefully dissolved in 50ml of methanol to create a homogeneous solution. This solution underwent the process of sonication and then was sequentially diluted with ethanol to achieve various concentrations: 2, 4, 6, 8, 10, 12, 14, 16, 18, and 20µg/ml. The absorbance levels of these different dilutions were meticulously measured at 254.0 nm against a blank sample utilizing a double beam UV spectrophotometer. Following this, a graph illustrating the relationship between absorbance and concentration in µg/mL was meticulously plotted. Finally, the obtained data was meticulously analyzed using linear regression analysis through Microsoft Excel.

Entrapment Efficiency (EE):

% EE: One millilitre of the freshly prepared SLN sample was carefully transferred into a sterile centrifuge tube. It was then subjected to centrifugation in a cooling centrifuge operating at a temperature of 4ºC. The centrifugation process lasted for 45 min. at a speed of 18000 revolutions per min. (rpm). After centrifugation, the centrifuge tube was removed, and the resultant supernatant was meticulously collected. Subsequently, the supernatant was subjected to analysis using a UV-visible spectrophotometer to estimate the sample's unentrapped drug. The % entrapment efficiency, a crucial parameter for assessing the effectiveness of drug encapsulation within SLNs, was calculated utilizing a specified formula to determine the percentage of drug successfully encapsulated within the nanoparticles.

$$\% \text{ EE} = \frac{\text{Total Drug Content - Unentrapped Drug}}{\text{Total Drug Content}} \times 100$$

Table 1: Entrapment Efficiency of the Prepared SLN

Runs (Batches)	% Entrapment Efficiency
1.	68.1±0.975
2.	56.9±1.282
3.	82.3±0.969
4.	93.5±0.827
5.	82.4±1.164
6.	68.4±0.993
7.	65±1.179
8.	85.1±0.938
9.	89.3±0.941
10.	82.4±1.172
11.	82.1±1.206
12.	93.7±0.893
13.	84±1.211

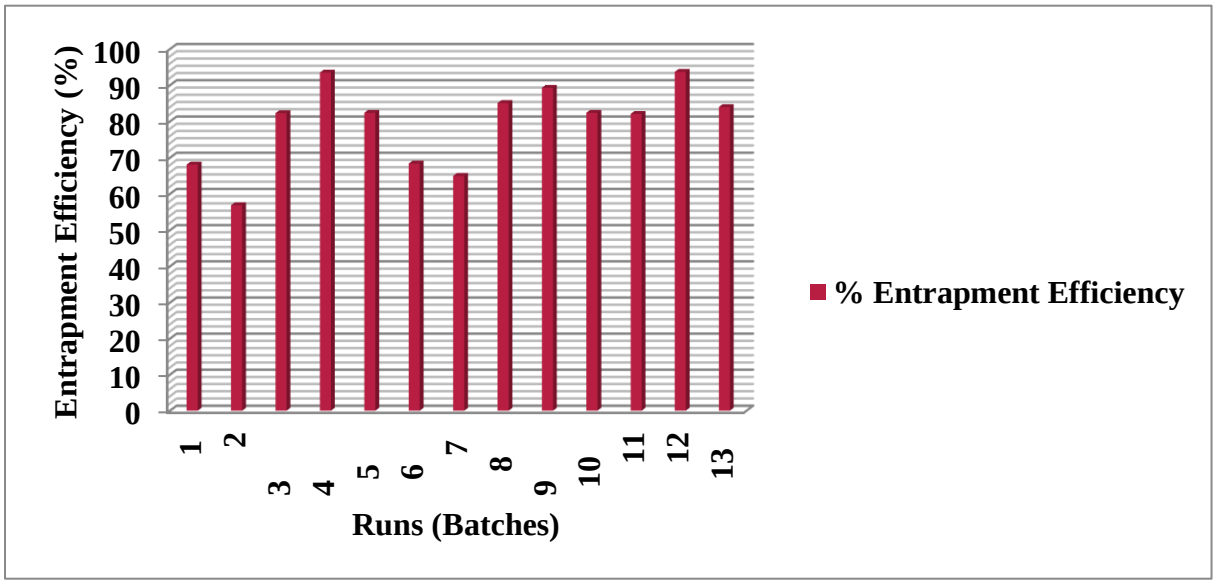

Figure 3: Entrapment Efficiency of the prepared SLN Entrapped with Essential Oil

In vitro evaporation release: To accurately evaluate chemical stability of the constituents in both pure medication and formed SLN, a comprehensive experimental protocol was implemented. The samples were meticulously placed in open vials and subjected to specific storage conditions, specifically being kept at a temperature of 35°C for duration of 6 days. During this experiment, materials were immersed in dehydrated alcohol for 30 minutes in an ultrasound chamber to extract essential oils. The selected elements were analyzed using the widely used Gas Chromatography (GC) method. The experimental groups used for comparison purposes included the Pure Drug group and the formulated SLN group with each group contributing valuable data to check the chemical stability of the samples under investigation.

Percent Drug Release: The drug liberates practices of both the pure drug and SLN was carefully examined using the USP dissolution apparatus Type I, which is a basket type apparatus. To enhance accuracy, the dissolution behavior of the optimized formulation of SLN and pure oil was scrutinized under the influence of phosphate buffer at pH 6.3 as the

dissolution medium. For the experimental procedure, a dialysis membrane encapsulating 1000 mg of the drug was first soaked overnight in the phosphate buffer solution with a pH of 6.3. Subsequently, the tightly tied dialysis membrane was placed within the basket of the apparatus, which was then filled with 900 ml of the pH 6.3 solution and left undisturbed for a period of 8 hours. At predetermined intervals throughout the 8 hours, 5ml samples were extracted and subsequently diluted with the phosphate buffer solution at pH 6.3. Ensuring accuracy and consistency, each time a sample was drawn, the apparatus was replenished with fresh dissolution medium, maintaining the sink condition. For further analysis, the diluted samples were subjected to UV-spectrophotometry at a wavelength of 254.0 nm to evaluate the drug release profiles at different time points.

3. RESULTS

Result: The spectrum of essential oil pure drug (Fig 4.) was found concordant with the reference spectrum of essential oil given in Fig 5. The characteristic peaks of essential oil are shown in Table No.1. The FTIR b spectrum of prepared SLN is shown in Fig No. 6 and characteristics peaks are shown in Table No: 2 which reveal that that was no mismatch, disappearance of the peaks

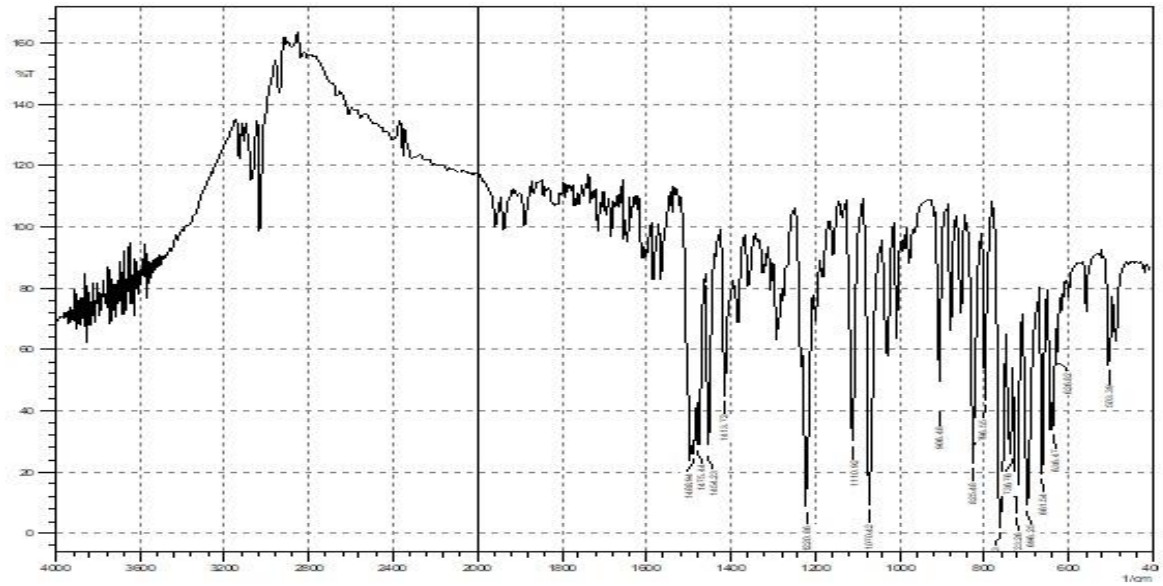

Figure 4: FTIR Spectrum of Pure Drug

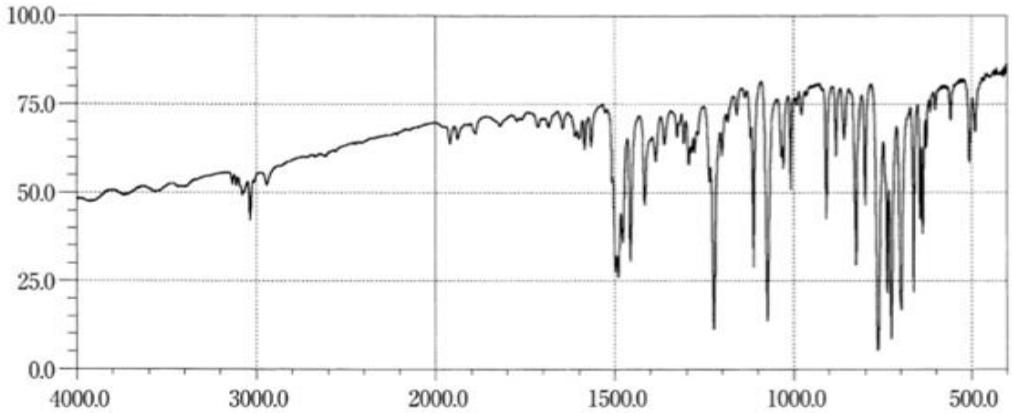

Figure 5: Reference FTIR Spectrum of Essential Oil

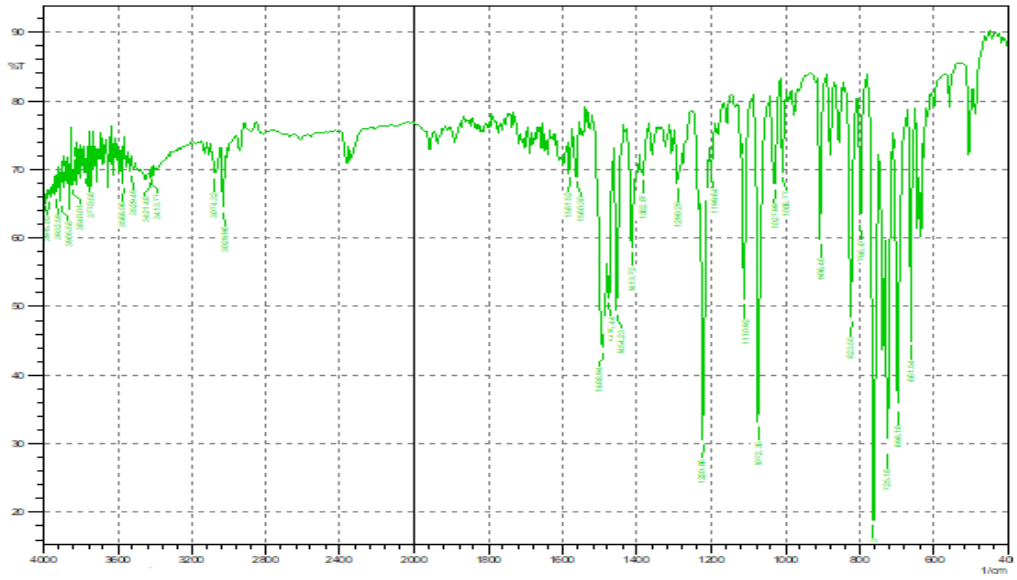

Figure 6: FTIR Spectrum of Prepared SLN

Table 2: Characteristic peaks of Essential Oil pure drug in FTIR spectrum

Frequency (cm^{-1})	Assignment
3029.96	Aromatic C-H stretching
2950	Aliphatic C-H stretching
1581.52	Aromatic C=C stretching
1454.23	Scissoring of C-H
1072.36	In plane C-H deformation
761.83 & 725.18	OOP C-H deformation

Table 3: Characteristics peaks of Prepared SLN

Frequency (cm^{-1})	Assignment
3529.49-3421.48	O-H stretching
3029.96	Aromatic C-H stretching
2950	Aliphatic C-H stretching
1581.52	Aromatic C=C stretching
1481.52	Scissoring of C-H
1072.36	In plane C-H deformation

761.83 & 725.18	**OOP C-H deformation**

Results: The Essential Oil exhibited excellent thermodynamic stability when subjected to temperatures of up to 300ºC during testing. Furthermore, when analyzing the melting curves of the DSC at a heating rate of 10 and 10ºC/min, no significant changes were detected. Lack to shift may be due to the evaporation of the solvent from the SLN during the preparation process. Consequently, the SLN samples prepared using chloroform demonstrated remarkable stability, as evidenced by the absence of distinct peaks in the melting points observed in the DSC results.

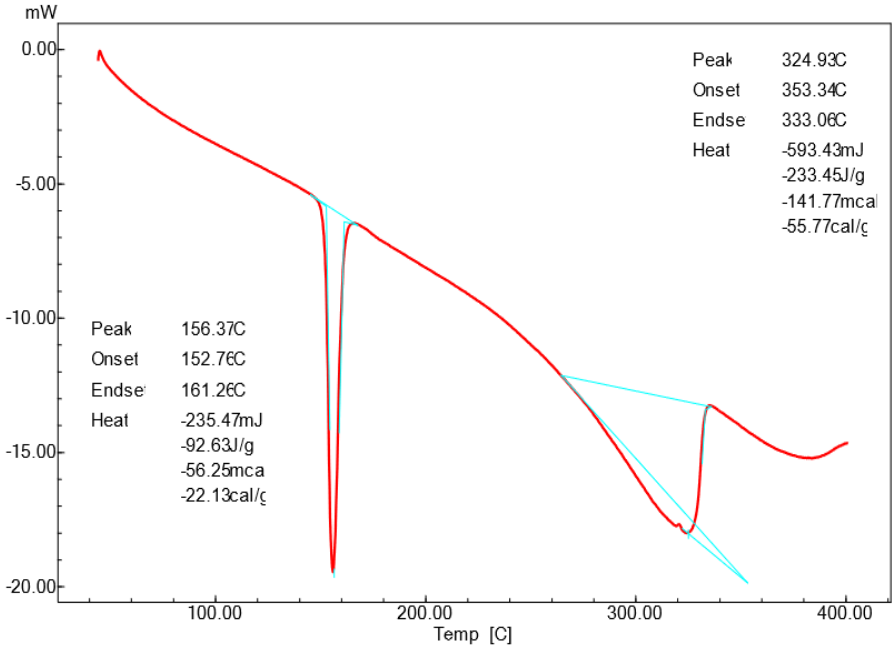

Figure No.7: DSC thermogram of Essential Oil pure drug

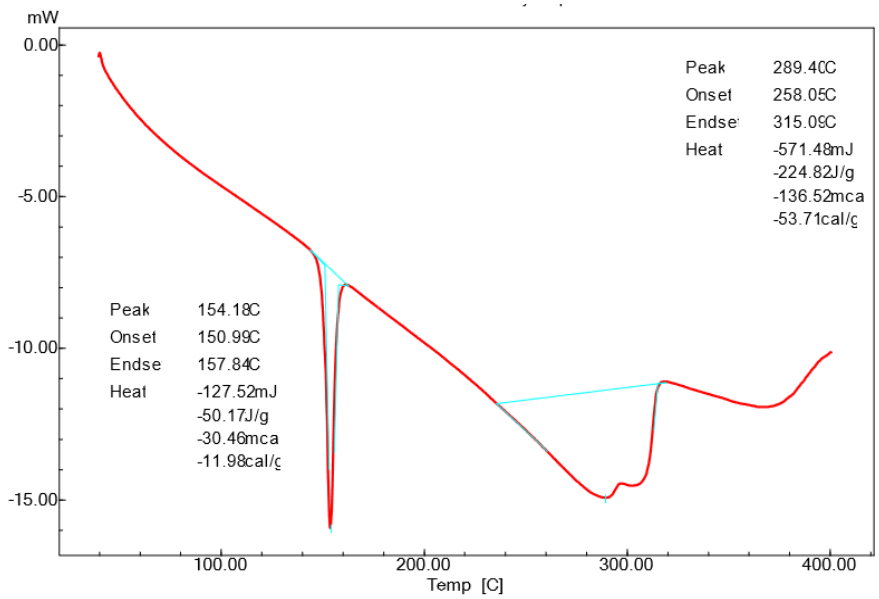

Figure No. 8: DSC thermogram of Essential Oil Entrapped in SLN

Result: XRD stands out as the most effective tool when it comes to identifying the drug entrapment within a specific formulation. The initial utilization of XRD was vital in validating the conclusions reached through DSC analysis. By examining the X-ray patterns of excipients combined with the drug, namely essential oil, the results from the XRD analysis unequivocally showed a consistent absence of peak discrepancies across a wide 2θ range of 2°–50°. This clear and

unambiguous observation solidifies the understanding that the drug has indeed been successfully encapsulated within the lipid core of the formulation.

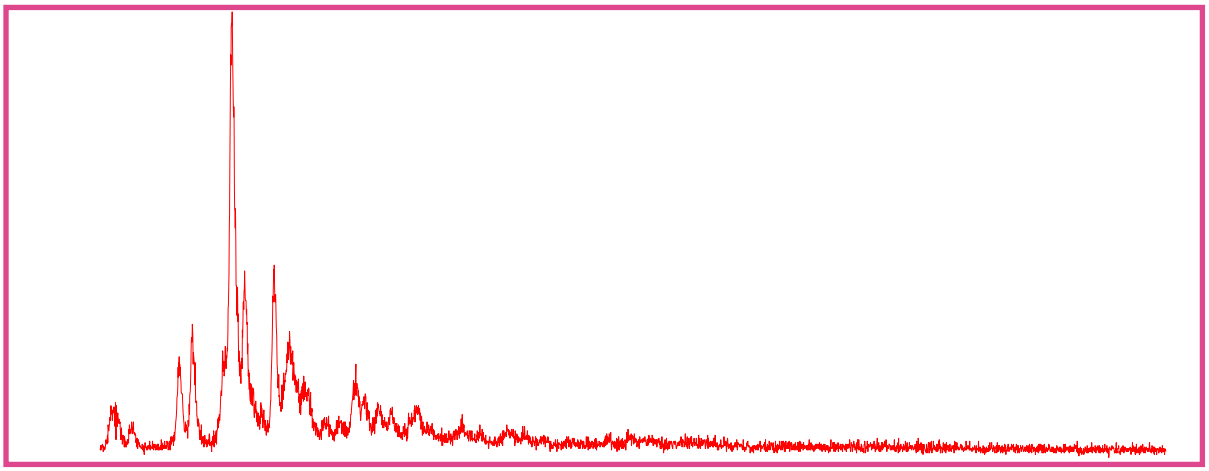

Figure No. 9: XRD of Pure Essential Oil

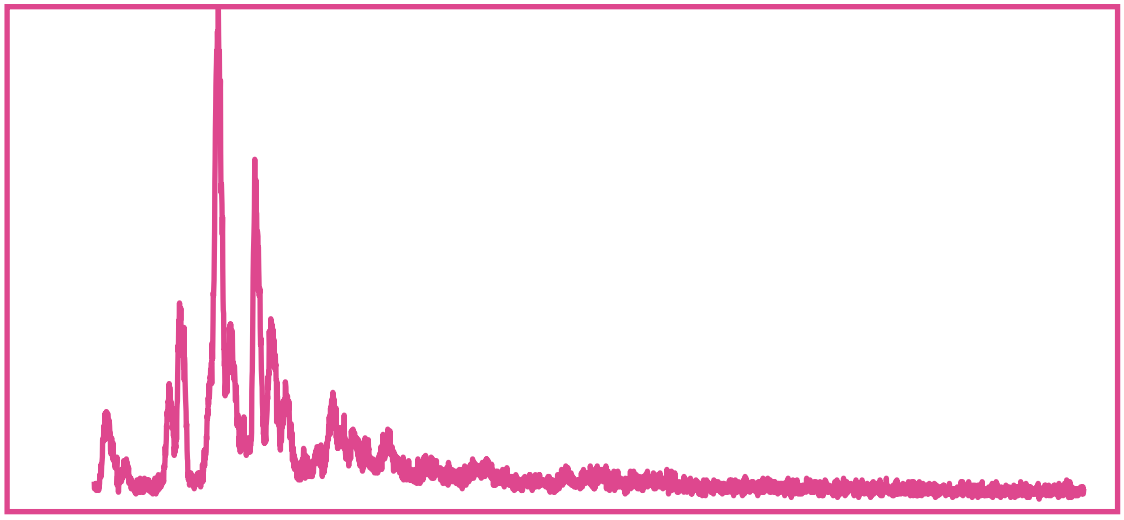

Figure No.10: XRD of Prepared SLN Entrapped with Essential Oil

Table 4: Peak data list of Essential Oil pure drug

no.	(deg)	(A)		(deg)	(Counts)	(Counts)
1	10.8600	8.14016	9	0.57000	34	739
2	11.1400	7.93618	7	0.54000	25	555
3	12.1200	7.29659	5	0.44000	18	447
4	15.2300	5.81289	19	0.38000	69	1484
5	16.0920	5.50340	26	0.36940	94	1881
6	16.5200	5.36177	4	0.08000	15	133
7	17.9200	4.94591	9	0.24000	33	1011

8	18.6886	4.74420	100	0.42030	362	8433
9	19.5089	4.54653	35	0.42790	127	3173
10	20.1000	4.41414	7	0.29340	27	570
11	20.6100	4.30604	4	0.30000	15	252
12	21.4504	4.13920	37	0.35420	134	2432
13	22.4200	3.96234	20	0.72000	73	2703
14	22.8800	3.88370	12	0.00000	42	0
15	23.4200	3.79536	9	0.86000	34	1718
16	26.7666	3.32794	11	0.46670	40	1010
17	27.3633	3.25671	7	0.43330	26	544
18	28.2900	3.15210	5	0.38000	18	395
19	29.1200	3.06412	5	0.28000	17	318
20	30.4000	2.93795	4	0.26660	15	196
21	30.7866	2.90194	7	0.61330	24	774
22	33.7400	2.65437	4	0.32000	13	396
23	36.7450	2.44390	3	0.35000	11	337

Table 5: Peak data list of Prepared SLN Entrapped with Essential Oil

Peak No.	2Θ (deg)	D (A)	I/I1	FWHM (deg)	Intensity (Counts)	Integrated (Counts)
1	10.9450	8.07713	14	0.75000	45	1774
2	12.2050	7.24596	5	0.47000	15	382
3	15.3533	5.76648	20	0.54670	67	1885
4	16.1596	5.48053	37	0.61420	123	3666
5	17.9600	4.93498	11	0.26000	36	808
6	18.7622	4.72575	100	0.60980	330	9975
7	19.6400	4.51647	30	0.82000	99	4027
8	20.5600	4.31640	6	0.57340	21	725
9	21.4721	4.13507	61	0.55290	201	5627

10	22.5900	3.93290	31	0.68400	101	3540
11	23.5858	3.76906	16	0.67830	54	2026
12	25.7800	3.45302	4	0.40000	12	238
13	26.8500	3.31779	14	0.62000	45	1272
14	27.5000	3.24083	8	0.56000	26	688
15	28.3250	3.14829	7	0.55000	23	680
16	29.2700	3.04876	4	0.30000	12	238
17	30.7650	2.90393	7	0.63000	22	975
18	37.8200	2.37686	4	0.40000	13	492
19	43.3500	2.08560	3	0.50000	10	362

Results: Upon examination using SEM and TEM, it was observed that the SLNs exhibited consistent morphologies. Figures 11, 12 and 13 illustrate that a majority of the particles possessed a spherical shape and displayed uniformity in size across samples. Notably, no substantial variations were detected in the structural characteristics of the SLNs. Detailed analysis of the photomicrographs captured through SEM and TEM revealed a well-defined spherical structure for the SLNs, with distinct angular features. Upon closer inspection at higher magnifications, the surfaces of these SLNs were observed to exhibit a smooth, spherical appearance. This uniformity in shape and size is likely attributed to the specific manufacturing processes that were employed during production. Furthermore, it was noted that there were no significant deviations in the morphology and appearance of other SLNs acquired from the chloroform extraction. Collectively, these findings suggest a consistent and reproducible nature in the morphology of the SLNs studied.

Figure No. 11: SEM of Prepared SLN at 1K Magnification

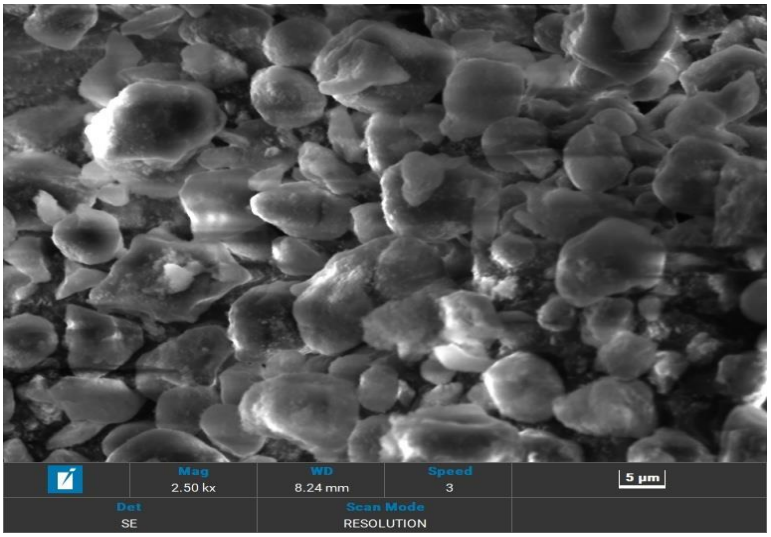

Figure No. 12: SEM of Prepared SLN at 2.5 K Magnifications

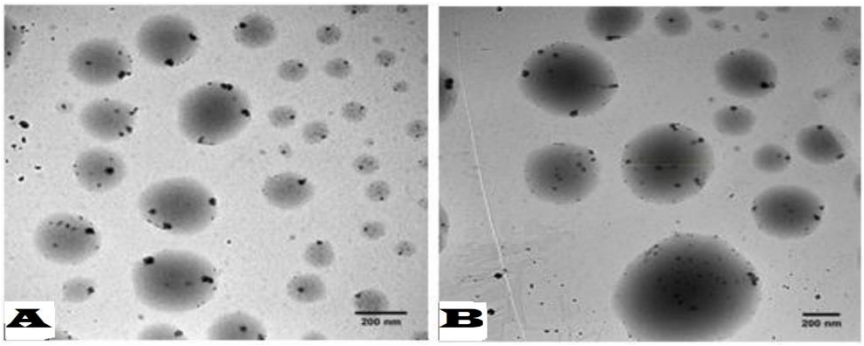

Figure No. 13: TEM of Prepared SLN (A is Magnification at 100 Times and B is Magnification at 200 times)

Results: The average SLN particle size was 189-780nm. Optimal formulation size in range was 200-250. The study found that increasing surfactant concentration led to smaller particle sizes due to decreased surface tension and surfaces free energy. Surfactant also prevented aggregate formation by breaking down melted lipid droplets, resulting in a stable dispersion. However, excess surfactant concentration increased particle size, possibly due to the surfactant surrounding lipid droplets. The zeta potential reveals the stability of the formulation which was found to be in the range of -22.6 to -68.5 mv. The research indicated that a PDI close to 0 is appropriate for a uniform distribution of SLNs and is deemed appropriate up to 0.5 for a narrow size distribution. However, increasing surfactant concentration decreased the PDI, possibly due to particle size differences. The PDI remained almost constant.

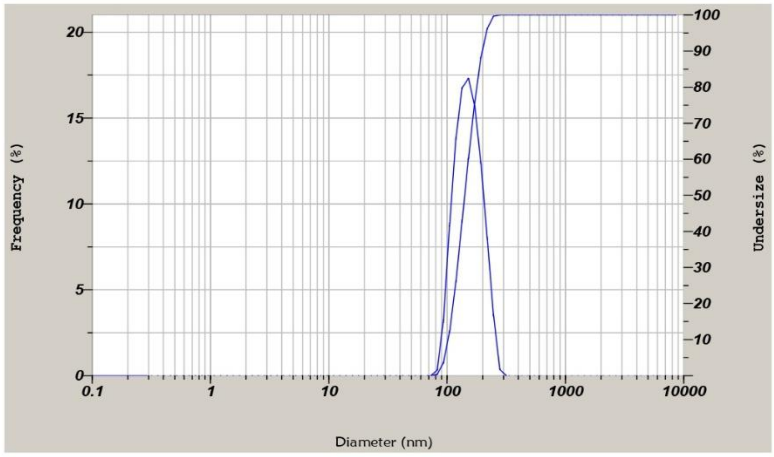

Figure No. 14: Particle Size of the Prepared SLN of Optimized Formulation

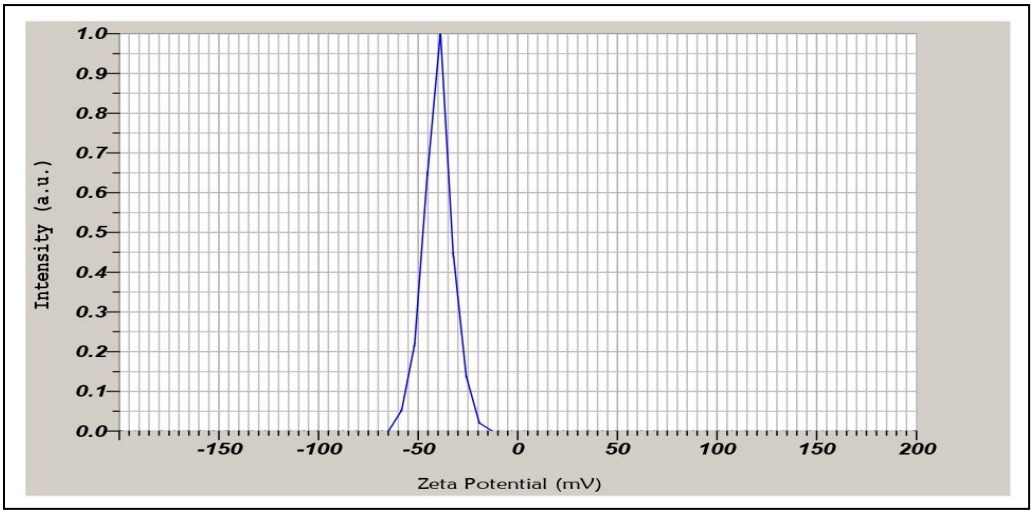

Figure No. 15: Zeta Potential of the Prepared SLN of Optimized Formulation

Result: Methanol was used for formation of SLN for solubilization of essential oil. Methanol retained in HS-GC at 2.87 min, 3.09 min and 3.19 min respectively. Fig No. 16 and 17 did not reveal the residual solvent peak and hence the entrapment of solvent during the formation of SLN from methanol. Hence it can be concluded that SLN formed by solvent evaporation technique of essential oil from methanol does not produce residual solvent toxicity in humans.

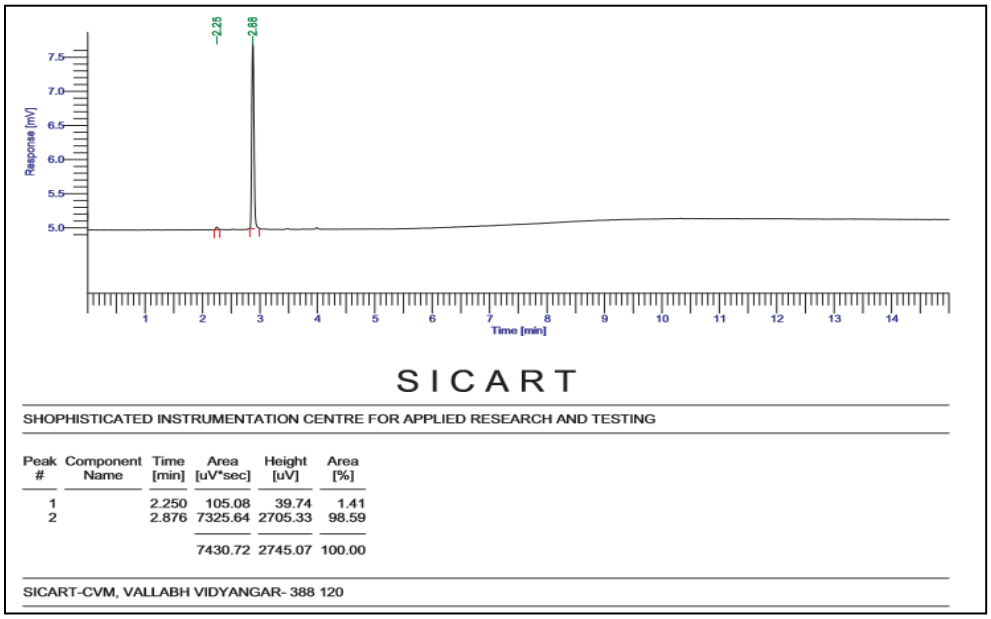

Figure No. 16: HS-GC of standard methanol solvent

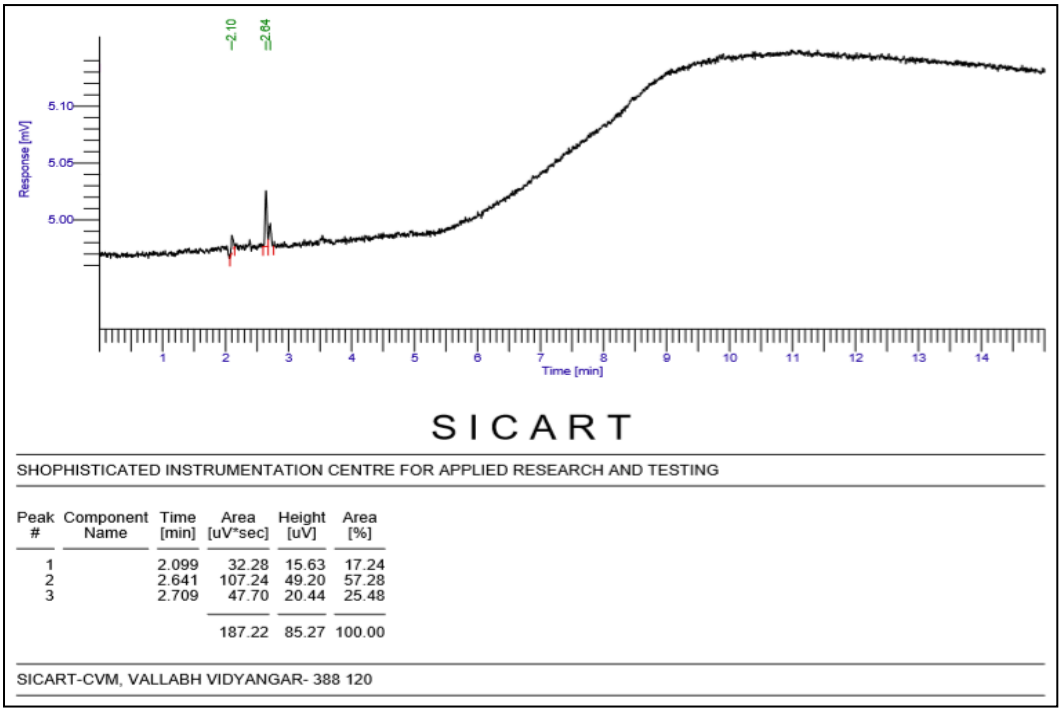

Figure No. 17: HS-GC of prepared SLN entrapped with Essential Oil

Result: The data exhibited a correction coefficient (R^2) of 0.9981, and the formula of the regressed line is shown as follows Y= 0.0577X + 0.0711 and Correlation coefficient (R^2) value indicates the linear correlation between concentration and absorbance. Thus, the method could be used successfully for analysis of Essential Oil content entrapped in SLN.

Table 6: Absorbance in Methanol at 254 nm

Sr. No.	Concentration (µg/ml)	Absorbance*
1	2	0.202 ± (0.0025)
2	4	0.294 ± (0.0013)
3	6	0.412 ± (0.0015)
4	8	0.530 ± (0.0055)
5	10	0.633 ± (0.0008)
6	12	0.772 ± (0.0011)
7	14	0.887 ± (0.0037)
8	16	1.058 ± (0.0048)
9	18	1.186 ± (0.0091)
10	20	1.332 ± (0.0018)

***Values are represented as mean ± SD, (n=3)**

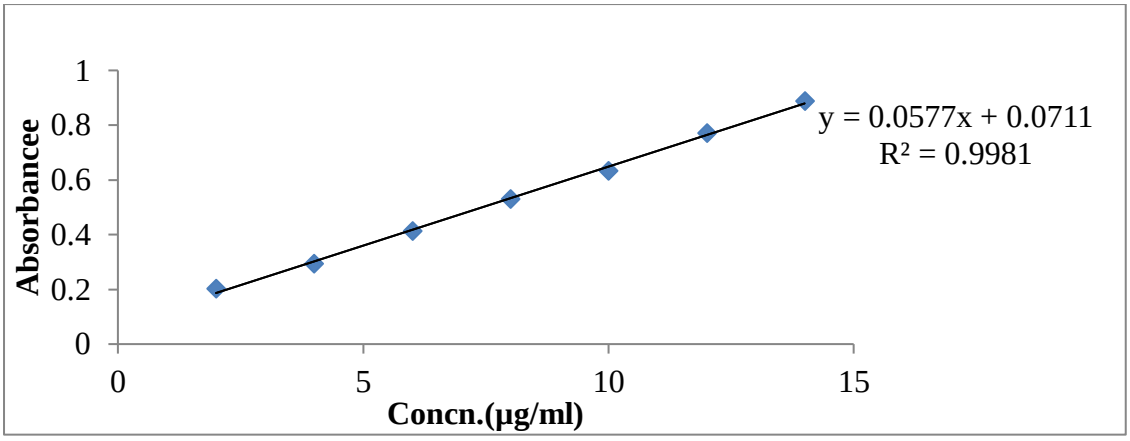

Figure 18: Standard Calibration Curve of Essential Oil

Result: Essential oils are volatile; therefore air, light, and high temperatures promote evaporation which damages active components, reducing activity. SLNs are more stable with essential oils, according to several research. The indexed components were six components with various boiling points according to the GC spectra to test SLNs' capacity to prevent essential oil evaporation. Evaporation release behavior of pure medication was standardised. Table 7 presents the findings for the in vitro evaporation release of the Pure Drug group and the compounded SLN group. Table 7 shows that all six components of the pure drug evaporate quickly, starting on the second day and reaching 50% losses after six days (excluding component 4). The formulated SLN (Table 7) shows a substantial decrease in evaporation loss compared to the pure drugs, with no component losing more than 50% after 6 days of storage, indicating that essential oil in SLN effectively reduces component evaporation loss.

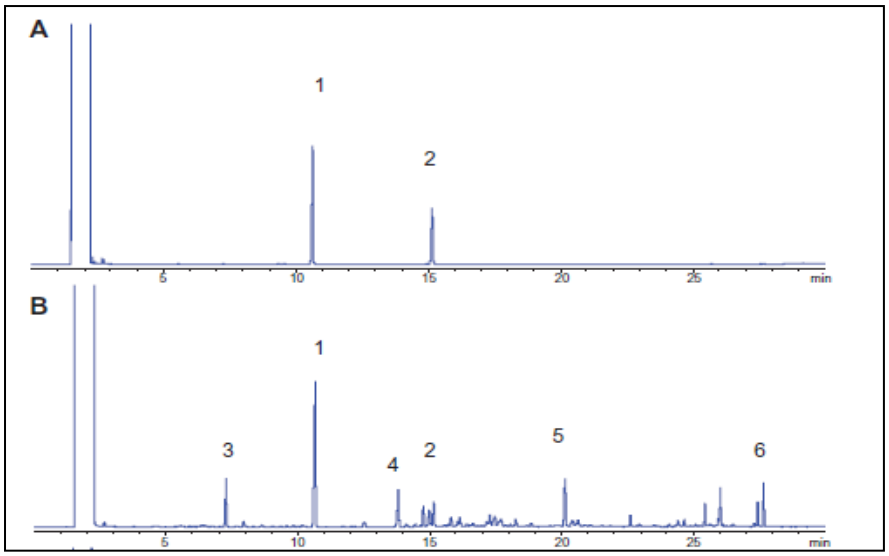

Figure 19: GC Analysis of Pure Drug and Prepared SLN

Table 7: Results of Components during Evaporation Study of Pure essential Oil and Prepared SLN entrapped with Essential Oil

Evaporation Study of Pure essential Oil						
Days	**Component 1**	**Component 2**	**Component 3**	**Component 4**	**Component 5**	**Component 6**
1	**0**	**0**	**0**	**0**	**0**	**0**
2	**12.21**	**12.49**	**13.41**	**5.21**	**28.47**	**49.02**
3	**19.89**	**18.59**	**18.15**	**19.58**	**32.59**	**54.98**

4	**26.29**	**25.30**	**25.68**	**23.24**	**38.95**	**58.05**
5	**38.57**	**37.31**	**36.79**	**34.24**	**48.55**	**64.04**
6	**50.89**	**50.09**	**49.85**	**46.16**	**59.18**	**70.94**
Evaporation Study of SLN entrapped with Pure essential Oil						
Days	**Component 1**	**Component 2**	**Component 3**	**Component 4**	**Component 5**	**Component 6**
1	**0**	**0**	**0**	**0**	**0**	**0**
2	**8.31**	**6.84**	**4.59**	**7.21**	**7.48**	**4.56**
3	**20.04**	**13.83**	**11.21**	**15.49**	**15.26**	**8.45**
4	**28.45**	**20.85**	**17.48**	**18.78**	**19.75**	**11.94**
5	**37.61**	**24.48**	**21.54**	**23.4**	**21.61**	**14.68**
6	**44.48**	**31.08**	**21.98**	**26.35**	**26.43**	**15.04**

Result: The drug release study spanned a duration of 12 hours. During this period, it was observed that the plain drug formulation released an impressive 96.89% of its contents within just 8 hours. In stark contrast, the optimized formulation exhibited a burst release of 20% within the initial 2 hours, followed by a consistent and sustained release profile that reached a remarkable 98.55% by the end of the 12-hour timeframe, as illustrated in Figure 18. These findings strongly support the notion that the specially prepared Solid Lipid Nanoparticles (SLN) can serve as a superior solution for achieving sustained and efficient drug delivery. By potentially reducing dosing frequency, this innovative system could offer enhanced therapeutic benefits and improved patient compliance in the long run. Optimized batch In-vitro Drug release was compared to Pure drug release.

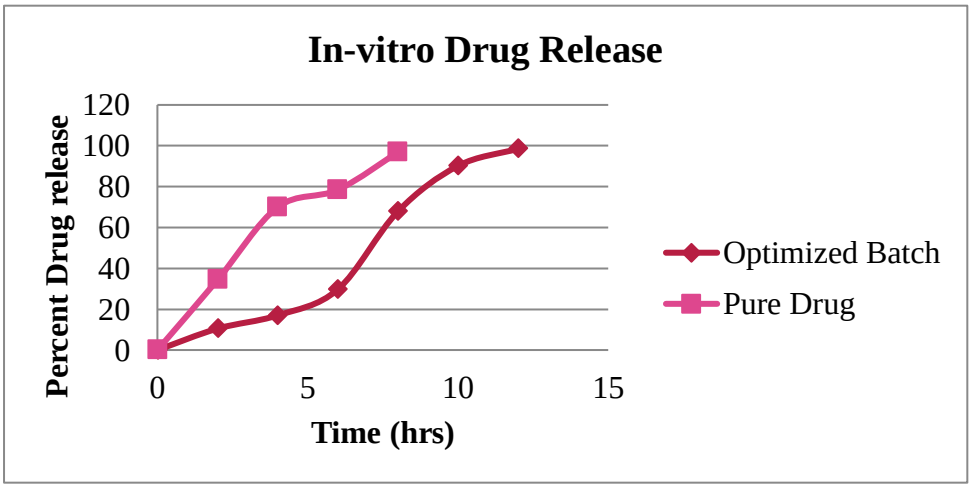

Figure 20: In-vitro Drug release (%)

Test samples were developed in preliminary research to determine preparation procedure feasibility. Phospholipid to Drug and Octa decyl amine ratios were tested for their effects on particle size and zeta emission with Lecithin to Cholesterol (1:0.5) and sonication time (12 minutes) 16-17 fixed.

Hydration of lipid films resulted in SLNs loaded with drugs. In a 500 ml round-bottom flask, 10 ml of chloroform was added to dissolve the precisely weighed lecithin, cholesterol, tristearin, and Octa decyl amine. In another container; correctly weighed drug was dispersed in a little amount of methanol. Both solutions were combined in round-bottom flask after dissolving. The inner wall of round bottom flask contains a thin dry layer from rotatory flash evaporation of volatile liquid. Overnight hydration with pH 7.4 PBS hydrated dry film. Sonication for 12 minutes produced vesicles of suitable size from milky dispersion after hydration. Sephadex G-50 column filtered dispersion to remove unformed vesicles and medication.

Experimental Design:

Box-behnken, a response surface design of experiment, was employed to optimize formulations by studying three components at three levels. Phospholipid to Drug ratio (A) and Phospholipid to Octa decyl amine ratio (B) were considered

at two levels (+1 and -1). All experiments were done in triplicate, and the average is used for evaluation. The optimal linear, two-factor connection, and quadratic model was determined using analysis of variance (ANOVA) and F-value, and a design with thirteen experiments, 8 non-center points, and 5 center points was created at the periphery of the design region to calculate the pure error sum of squares. Using design expert software (V-13.0), response surface three-dimensional (3-D) models and quadratic equations were used to study the effect of independent factors on dependent variables particle size (Y1) and Zeta potential (Y2).

Table 8: Variables and their levels in Box-Behnken design.

Variable Code	Variable	Coded values/actual values	
		+1	-1
A	Phospholipid to Drug (%w/w)	5 % (5mg)	1 % (1 mg)
B	Phospholipid to Octadecylamine ratio (%w/w)	15% (15 mg)	5% (5 mg)

Table 9: Formulation Chart according to the study.

Runs	Factor A Phospholipid to Drug	Factor B Phospholipid to Octadecylamine ratio	Response 1 Particle Size (nm)	Response 2 Zeta Potential (mv)
1	0	0	564	-52.1
2	0	-1.41421	189	-22.6
3	1.41421	0	678	-64.4
4	0	0	206	-56.4
5	-1	1	405	-57.4
6	0	1.41421	641	-55.8
7	0	0	488	-28.3
8	-1.41421	0	651	-66.8
9	1	1	492	-25.7
10	0	0	378	-42.3
11	-1	-1	432	-27.8
12	1	-1	489	-68.5
13	0	0	780	-59.3

Table 3 shows that after applying a quadratic model adjustment to Y1 and Y2, there was a substantial lack of fit for all variables ($P>0.05$). Individual and interaction effects of variables that are independent on dependent variables were explained by polynomial equations for each dependent variable. Positive polynomial equation signs indicate synergy, while negative indicators indicate dependent variable disagreement.

Table 10: Results of regression analysis for responses Y1 and Y2

Model	Sequential p-value	Lack of fit p-value	Adjusted R^2	Predicted R2	Remarks
Response (Particle Size, Y1)					
Linear	0.0004	0.0003	0.6774	0.5363	
2FI	0.8362	0.0002	0.6135	0.1119	
Quadratic	<0.0001	0.0525	0.9835	0.9025	Suggested
Response (Zeta Potential, Y2)					
Linear	<0.0001	0.0309	0.8505	0.7614	
2FI	0.8473	0.0184	0.8200	0.4877	
Quadratic	0.0053	0.1705	0.9539	0.7704	Suggested

Table 11: Fit Statistic for responses Y1 and Y2

Response	R2	Adjusted R2	Predicted R2	Adeq Precision	Std. Dev.	Mean	% CV
Particle Size (Y1)	0.9928	0.9835	0.9025	39.2891	20.41	466.35	4.38
Zeta Potential (Y2)	0.9798	0.9539	0.7704	17.7890	3.14	47.68	6.58

Table 12: Analysis of Variance (ANOVA) of calculated model for responses.

Result of the ANOVA	Particle Size (nm)	Zeta Potential (mV)
Regression		
Sum of Squares	4.013E + 05	3339.59
Degree of freedom (df)	9	9
Mean square	44583.44	371.07
F-value	106.99	37.75
p-value	<0.0001	<0.0001
Inference	Significant	Significant
Lack of fit tests		
Sum of squares	2413.75	46.76
Degree of freedom (df)	3	3
Mean square	804.58	15.59
F-value	6.40	2.83
p-value	0.0525	0.1705
Inference	Not significant	Not significant
Residual		
Sum of Squares	2916.95	68.81
Degree of freedom (df)	7	7
Mean square	416.71	9.83

Particle Size (Y1): A significant model F value of 106.99 (P<0.0001) for particle size. The non-significant lack of fit F-

value of 6.40 (P>0.05). So, model fit is good. R2=0.9928, polynomial equation correlation coefficient, showed significant data fitting in model. A reasonable agreement between the expected R2 of 0.9025 and the adjusted R2 of 0.9835 shows that the model can predict particle size response. Adeq precision assesses signal-to-noise ratio. A ratio over 4 is ideal. Adeq. Precision for particle size is 39.289, providing a good signal for design space navigation.

The second-order polynomial equation for particle size(Y1) response is below:

$$Y1 = 382.60 + 57.63A + 135.75B + 124.63C$$
$$-30.50AB + 18.25AC - 28.50BC$$
$$+ 98.58A^2 - 27.18B^2$$
$$+ 106.58C^2$$

In the quadratic equation, individual factors A, B, and C have synergistic effects, including compounded effects, but combined effects of A, B, and B, C have antagonistic effects on particle size. According to quadratic equation, particle size increases with factor values. Tristearin is Emulsomes' core material, so increasing the percentage of Bifonazole, Tristearin, and Stearyl amine may result in a bulkier core as more core is accumulated in Emulsome vesicles. Increased stearyl amine percentage increases charge on vesicles, which increases phospholipid bilayer repulsion and particle size. Figure 2: Particle size 3-D response surface plots.

Figure 2: 3-Dimensional reaction surface plots show the interaction effect of variables A & B (a), A & C(b), B & C (c) on particle size (Y1).

Zeta Potential (Y2):

In Tables 5 and 6, the model F value for size was 37.75 ($p < 0.0001$), indicating significance. The non-significant lack of fit F-value is 2.83 ($p > 0.05$). So model fit is good. Polynomial equation correlation coefficient ($R2 = 0.9798$) showed model data fitting. The model can predict zeta potential response because the expected R2 of 0.7704 matches the adjusted R2 of 0.9539. Adeq precision assesses signal-to-noise ratio. A ratio over 4 is ideal. Adeq precision for zeta potential is 17.789, providing a sufficient signal for design space navigation. The second-order polynomial equation for Zeta potential (Y2) response is below:

$$Y2= 45.08 - 0.2875A - 0.8625B + 19.33C$$
$$+0.6750AB - 2.00AC - 1.80BC$$
$$+5.30A^2 + 5.05B^2 - 4.83C^2$$

In quadratic equation, each factor C and combination factors AB synergistically affect Zeta potential, while every factor A, B and their combined components A, C and B, C antagonistically affect it. Stearyl amine induces vesicle charges, which may explain why factor C enhances Zeta potential.

Figure 21: Zeta potential (Y2) 3-D response surface plots.

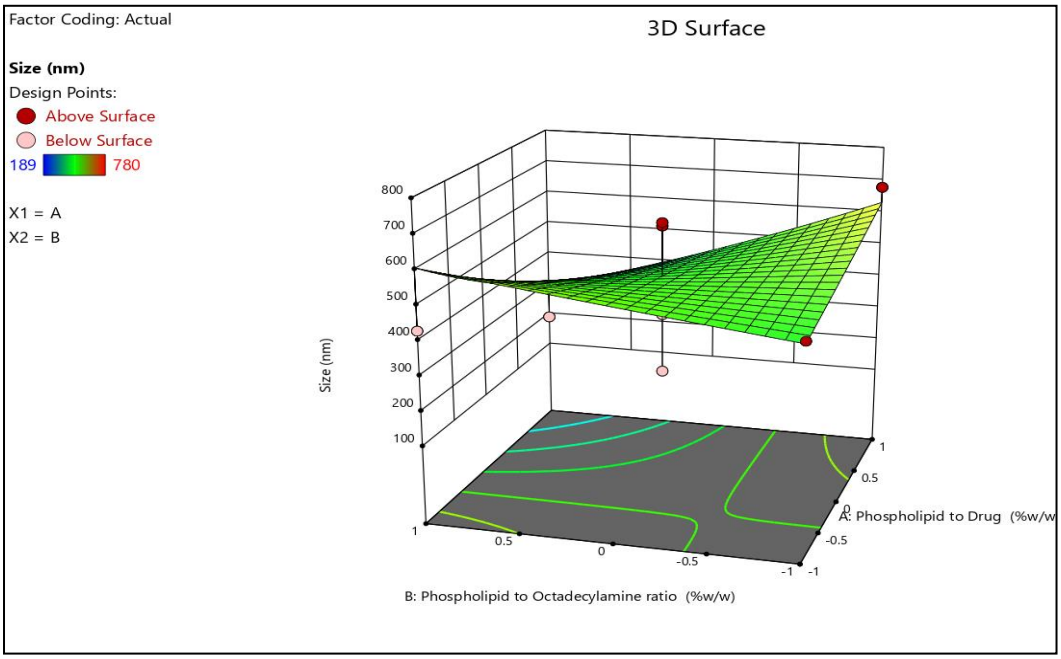

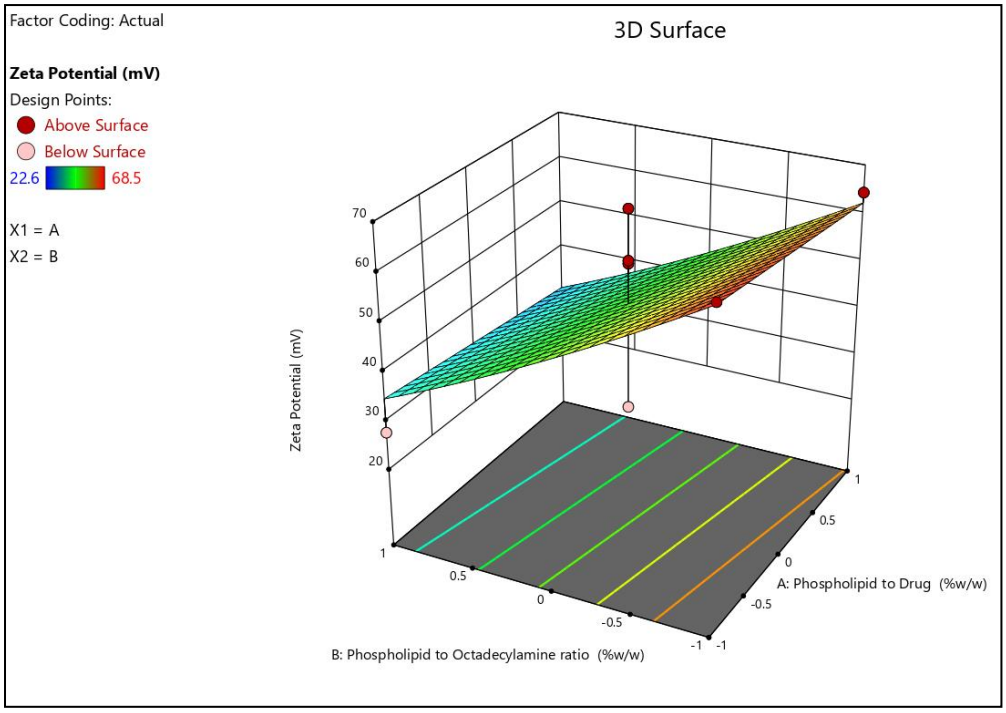
Factor Coding: Actual
Zeta Potential (mV)
Design Points:
Above Surface
Below Surface
22.6
68.5
X1 = A
X2 = B
3D Surface
Zeta Potential (mV)
70
60
50
40
30
20
1
0.5
0
-0.5
-1
B: Phospholipid to Octadecylamine ratio (%w/w)
A: Phospholipid to Drug (%w/w)

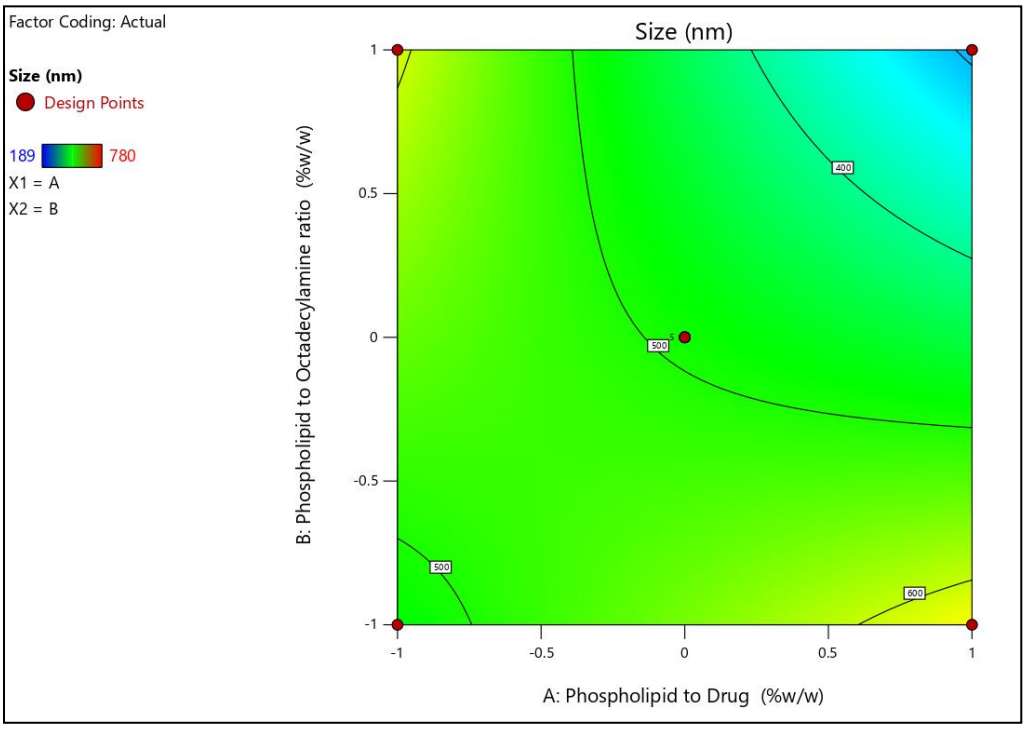
Factor Coding: Actual
Size (nm)
Design Points
189
780
X1 = A
X2 = B
Size (nm)
B: Phospholipid to Octadecylamine ratio (%w/w)
A: Phospholipid to Drug (%w/w)
400
500
500
600
1
0.5
0
-0.5
-1

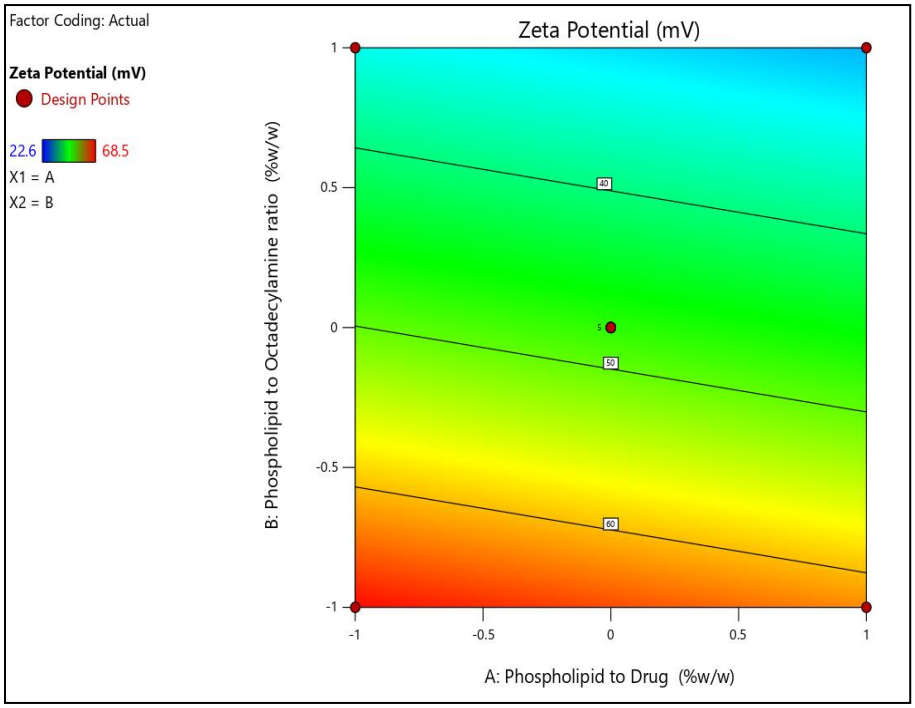

4. CONCLUSION

This study highlights the successful development and characterization of SLNPs encapsulating BEO to enhance its stability, controlled release, and therapeutic potential. BEO, despite its well-known antimicrobial, antioxidant, and anti-inflammatory properties, faces significant challenges such as high volatility, low solubility, and susceptibility to environmental degradation. The use of SLNPs effectively addresses these limitations, offering improved bioavailability and protection from external factors.

Through a combination of heat homogenization and ultrasonication techniques, the SLNPs were formulated and evaluated based on parameters such as particle size, zeta potential, PDI, and encapsulation efficiency. Characterization studies, including FTIR and DSC, confirmed successful encapsulation and compatibility of BEO within the lipid matrix. Additionally, in vitro release studies demonstrated a prolonged release profile, significantly reducing the evaporation of volatile compounds, a critical limitation of free BEO. Furthermore, antimicrobial tests revealed that SLNP-loaded BEO exhibited enhanced efficacy against common pathogens compared to its free form. The sustained release from SLNPs allows prolonged interaction with microbial cells, contributing to improved antibacterial activity. Cytotoxicity evaluations confirmed the biocompatibility of the formulations, supporting their potential for safe therapeutic applications in the pharmaceutical and cosmetic industries.

The study also suggests that SLNPs could be a promising carrier system for essential oils in various applications, including food preservation, cosmetics, and pharmaceutical formulations. By protecting the bioactive components from degradation and ensuring controlled release, SLNPs offer a viable strategy for overcoming the inherent challenges associated with essential oil-based therapeutics. While these findings present a strong case for the use of SLNPs in BEO delivery, further in vivo investigations are needed to confirm their pharmacokinetic properties, therapeutic efficacy, and safety profile. Future research should focus on scaling up the formulation process, conducting long-term stability studies, and evaluating clinical effectiveness. The promising results from this study pave the way for the broader application of SLNP technology in developing novel drug delivery systems, particularly for natural bioactive compounds. This study reinforces the potential of SLNPs as a robust and efficient platform for enhancing the stability, bioavailability, and therapeutic impact of Bergamot Essential Oil, marking a significant advancement in the field of nanotechnology-driven drug delivery.

5. ACKNOWLEDGEMENT

I would like to share my gratitude to my guide Prof. Shantilal Singune sir and management of Institute of Pharmaceutical Sciences, SAGE University, Indore for their continuous support & Guidance.

REFERENCES

[1] Zhong G, Nicolosi E. Citrus origin, diffusion, and economic importance. The citrus genome. 2020:5-21.

[2] Calabrese F. La favolosa storia degli agrumi.

[3] Inglese P, Sortino G. Citrus history, taxonomy, breeding, and fruit quality. InOxford research Encyclopedia of environmental science 2019 Feb 25.

[4] Wu GA, Terol J, Ibanez V, López-García A, Pérez-Román E, Borredá C, Domingo C, Tadeo FR, Carbonell-Caballero J, Alonso R, Curk F. Genomics of the origin and evolution of Citrus. Nature. 2018 Feb;554(7692):311-6.

[5] Dugo G, Mondello L, editors. Citrus oils: composition, advanced analytical techniques, contaminants, and biological activity. CRC press; 2010 Nov 2.

[6] Zhong G, Nicolosi E. Citrus origin, diffusion, and economic importance. The citrus genome. 2020:5-21.

[7] Chase MW, Christenhusz MJ, Fay MF, Byng JW, Judd WS, Soltis DE, Mabberley DJ, Sennikov AN, Soltis PS, Stevens PF. An update of the Angiosperm Phylogeny Group classification for the orders and families of flowering plants: APG IV. Botanical journal of the Linnean Society. 2016 May 1;181(1):1-20.

[8] Dugo G, Di Giacomo A, editors. Citrus: the genus citrus. CRC Press; 2002 Sep 12.

[9] Goldschmidt EE. The Citrus genome: past, present and future. The Citrus Genome. 2020:1-3.

[10] Velasco R, Licciardello C. A genealogy of the citrus family. Nature biotechnology. 2014 Jul;32(7):640-2.

[11] Carbonell-Caballero J, Alonso R, Ibañez V, Terol J, Talon M, Dopazo J. A phylogenetic analysis of 34 chloroplast genomes elucidates the relationships between wild and domestic species within the genus Citrus. Molecular biology and evolution. 2015 Aug 1;32(8):2015-35.

[12] Carbonell-Caballero J, Alonso R, Ibañez V, Terol J, Talon M, Dopazo J. A phylogenetic analysis of 34 chloroplast genomes elucidates the relationships between wild and domestic species within the genus Citrus. Molecular biology and evolution. 2015 Aug 1;32(8):2015-35.

[13] Wu GA, Prochnik S, Jenkins J, Salse J, Hellsten U, Murat F, Perrier X, Ruiz M, Scalabrin S, Terol J, Takita MA. Sequencing of diverse mandarin, pummelo and orange genomes reveals complex history of admixture during citrus domestication. Nature biotechnology. 2014 Jul;32(7):656-62.

[14] Schwartz T, Nylinder S, Ramadugu C, Antonelli A, Pfeil BE. The origin of oranges: a multi-locus phylogeny of Rutaceae subfamily Aurantioideae. Systematic Botany. 2016 Jan 1;40(4):1053-62.

[15] Curk F, Ollitrault F, Garcia-Lor A, Luro F, Navarro L, Ollitrault P. Phylogenetic origin of limes and lemons revealed by cytoplasmic and nuclear markers. Annals of botany. 2016 Apr 1;117(4):565-83.

[16] Federici CT, Roose ML, Scora RW. RFLP analysis of the origin of Citrus bergamia, Citrus jambhiri, and Citrus limonia. InFirst International Citrus Biotechnology Symposium 535 1998 Nov 29 (pp. 55-64).

[17] Nicolosi E, Deng ZN, Gentile A, La Malfa S, Continella G, Tribulato E. Citrus phylogeny and genetic origin of important species as investigated by molecular markers. Theoretical and Applied Genetics. 2000 Jun;100:1155-66.

[18] Li X, Xie R, Lu Z, Zhou Z. The origin of cultivated citrus as inferred from internal transcribed spacer and chloroplast DNA sequence and amplified fragment length polymorphism fingerprints. Journal of the American Society for Horticultural Science. 2010 Jul 1;135(4):341-50.

[19] Maruca G, Laghetti G, Mafrica R, Turiano D, Hammer K. The Fascinating History of Bergamot (Citrus Bergamia Risso & Poiteau), the Exclusive Essence of Calabria: A.

[20] Navarra M, Mannucci C, Delbò M, Calapai G. Citrus bergamia essential oil: from basic research to clinical application. Frontiers in pharmacology. 2015 Mar 2;6:36.

[21] Solans C, Izquierdo P, Nolla J, Azemar N, Garcia-Celma MJ. Nano-emulsions. Current opinion in colloid & interface science. 2005 Oct 1;10(3-4):102-10.

[22] Shah P, Bhalodia D, Shelat P. Nanoemulsion: A pharmaceutical review. Systematic reviews in pharmacy. 2010 Jan 1;1(1).

[23] Becher P. Emulsions: theory and practice. Washington, DC: American Chemical Society; 2001 Jan.

[24] Slomkowski S, Alemán JV, Gilbert RG, Hess M, Horie K, Jones RG, Kubisa P, Meisel I, Mormann W, Penczek S, Stepto RF. Terminology of polymers and polymerization processes in dispersed systems (IUPAC Recommendations 2011). Pure and Applied Chemistry. 2011 Sep 10;83(12):2229-59.

[25] de Oliveira Filho JG, Miranda M, Ferreira MD, Plotto A. Nanoemulsions as edible coatings: a potential strategy for fresh fruits and vegetables preservation. Foods. 2021 Oct 14;10(10):2438.

[26] Jampilek J, Kos J, Kralova K. Potential of nanomaterial applications in dietary supplements and foods for special medical purposes. Nanomaterials. 2019 Feb 19;9(2):296.

[27] Jampilek J, Kralova K. Potential of nanonutraceuticals in increasing immunity. Nanomaterials. 2020 Nov 9;10(11):2224.

[28] Akbarzadeh A, Rezaei-Sadabady R, Davaran S, Joo SW, Zarghami N, Hanifehpour Y, Samiei M, Kouhi M, Nejati-Koshki K. Liposome: classification, preparation, and applications. Nanoscale research letters. 2013 Dec;8:1-9.

[29] Filipczak N, Pan J, Yalamarty SS, Torchilin VP. Recent advancements in liposome technology. Advanced drug delivery reviews. 2020 Jan 1;156:4-22.

[30] Andra VV, Pammi SV, Bhatraju LV, Ruddaraju LK. A comprehensive review on novel liposomal methodologies, commercial formulations, clinical trials and patents. Bionanoscience. 2022 Mar;12(1):274-91.

[31] Khairnar SV, Pagare P, Thakre A, Nambiar AR, Junnuthula V, Abraham MC, Kolimi P, Nyavanandi D, Dyawanapelly S. Review on the scale-up methods for the preparation of solid lipid nanoparticles. Pharmaceutics. 2022 Sep 6;14(9):1886.

[32] Muller H. R.; Shegokar, R.; M Keck, C. 20 years of lipid nanoparticles (SLN & NLC): Present state of development & industrial applications. Curr. Drug Discov. Technol. 2011;8(3):207-27.

[33] Elkordy AA, Haj-Ahmad RR, Awaad AS, Zaki RM. An overview on natural product drug formulations from conventional medicines to nanomedicines: Past, present and future. Journal of Drug Delivery Science and Technology. 2021 Jun 1;63:102459.

[34] Gupta S, Tejavath KK. Nano phytoceuticals: A step forward in tracking down paths for therapy against pancreatic ductal adenocarcinoma. Journal of Cluster Science. 2022:1-21.

[35] Yap KM, Sekar M, Fuloria S, Wu YS, Gan SH, Mat Rani NN, Subramaniyan V, Kokare C, Lum PT, Begum MY, Mani S. Drug delivery of natural products through nanocarriers for effective breast cancer therapy: A comprehensive review of literature. International Journal of Nanomedicine. 2021 Dec 2:7891-941.